Acta Materialia 122 (2017) 431–437

Contents lists available at ScienceDirect

Acta Materialia

journal homepage: www.elsevier.com/locate/actamat

Full length article

Solidification velocity of undercooled Fe–Co alloys

Justin E. Rodriguez [a, *], Carolina Kreischer [b], Thomas Volkmann [b], Douglas M. Matson [a]

[a] Department of Mechanical Engineering, Tufts University, Medford, MA 02155, USA
[b] Institut für Materialphysik im Weltraum, Deutsches Zentrum für Luft- und Raumfahrt (DLR), Linder Höhe, Cologne 51147, Germany

ARTICLE INFO

Article history:
Received 4 August 2016
Received in revised form
26 September 2016
Accepted 27 September 2016
Available online 14 October 2016

Keywords:
Containerless processing
Rapid solidification
Computational materials modeling
Iron-cobalt alloys

ABSTRACT

The goal of this work was to investigate intra-alloy relationships, as they pertain to rapid solidification, which can be applied to computational materials modeling. Those relationships can be utilized to improve the accuracy of predictive modeling by leveraging previous experimental results. With that in mind, Fe–Co samples were prepared with 30–50 at.% cobalt and they were processed via electrostatic levitation (ESL) or electromagnetic levitation (EML). The samples were levitated, melted, and allowed to cool and solidify in a vacuum for ESL testing and under He gas for EML testing. If sufficient undercooling was achieved, the sample solidified via double recalescence. In that event, the metastable δ–phase would grow into the undercooled liquid, and then the stable γ–phase would grow into a combination of the metastable phase and remaining undercooled liquid, or mushy zone. The velocities of the solid phases growing into undercooled liquid were analyzed with current dendrite growth theories. The purpose of the growth velocity analyses was two-fold: 1) Assess the validity of current dendrite theory as it applies to the Fe–Co system. 2) Evaluate the kinetic growth coefficient, μ, assuming a constant kinetic rate parameter, V_o. The results of the analyses indicate that it is reasonable to assume that the kinetic rate parameter, V_o, is constant for a given phase within an alloy system if $\Delta H_f/T_m^2$ does not vary significantly within the system, or within the composition range of interest. The average growth velocities of the stable phase into the mushy zone, $\overline{V}_{\gamma\delta}$, for the Fe–30, 40, and 50 at.% Co compositions are 1.6, 2.4, and 4.9 m/s, respectively, which scale with the thermal driving forces of the transformations, $\Delta T_{\gamma\delta}$, which are 10 K, 24 K, and 40 K, respectively.

1. Introduction

Containerless processing methods, such as electrostatic levitation (ESL), or electromagnetic levitation (EML), allow a molten sample to undercool below the stable γ–phase (FCC) liquidus temperature over a wide composition range for Iron-Cobalt alloys. If the undercooling is sufficient, i.e. the temperature is below the melting point of the metastable δ–phase (BCC), the sample can solidify in a two-step process known as double recalescence. In the event of double recalescence, dendrites of the metastable BCC δ–phase grow into the undercooled liquid, and the stable FCC γ–phase grows subsequently into the combination of primarily formed metastable solid and remaining undercooled liquid, or mushy zone [1–4].

Due to primary solidification of the δ–phase, the temperature is raised by the released heat of fusion to the solidification temperature located between liquidus and solidus temperature of the metastable phase. After a short delay time, nucleation and growth of the stable phase sets in and the temperature is further increased towards the equilibrium liquidus temperature by which the primary metastable phase is either remelted or transformed into the stable phase. Therefore, besides the delay time for nucleation the growth velocity of the stable phase in the mushy zones determines the dynamics of the metastable-stable phase transformation and is a decisive parameter controlling the formation of the microstructure.

Growth kinetics and microstructural evolution are generally influenced by fluid flow because it affects the heat and mass transport at the solid-liquid interface. The effect is more apparent the lower the growth rate is compared to the fluid flow speed [5]. Hermann et al. [2–4] reported Fe–Co growth velocity results for the γ–phase and metastable δ–phase growing through undercooled liquid, using EML processing in both terrestrial and microgravity conditions during parabolic flight; thus, different levels of

* Corresponding author. Tufts University 200 College Avenue, Medford, MA 02155, USA.
E-mail address: Rodrigu.Ju@gmail.com (J.E. Rodriguez).

http://dx.doi.org/10.1016/j.actamat.2016.09.047
1359-6454/

forced electromagnetic stirring were achieved [6]. In those experiments double recalescence was detected by a fast responding silicon photo diode. Growth velocity of the primary growing phase was inferred from temperature-time characteristics while growth kinetics of the secondary stable phase could not be obtained by this method. However, an effect of melt convection on primary growth kinetics could not be detected because the solidification velocities of the γ and δ phases were in the range of several m/s which is much larger than fluid flow velocities in EML processing on ground and under microgravity [6].

Li et al. [7] discussed microstructure and phase selection in undercooled Fe–30 at.% Co melts in the context of glass flux experiments and subsequent microscopical investigations on as-solidified samples but in-situ measurements during rapid solidification have not been carried out.

In this article, we report new experimental results of growth velocity from both electrostatically and electromagnetically levitated samples. While electromagnetic levitation processing leads to stirring in the melt, the electrostatic levitation technique provides containerless solidification experiments without induced convection [8]. In the current work, rapid solidification was monitored by high-speed video camera. Imaging of double recalescence enabled measurement of the velocity of the stable phase through the mushy zone of the primarily solidified metastable phase, as well as growth of the solid phases through undercooled liquid. The measured velocities as a function of undercooling for both of the stable γ–phase and metastable δ–phase are assessed using Lipton-Kurz-Trivedi (LKT) theory [9], including the kinetic undercooling component from Boettinger-Coriell-Trivedi (BCT) theory [10]. The purpose of the growth velocity analysis was two-fold: 1) Assess the validity of the theory as it applies to the Fe–Co system. 2) Evaluate the kinetic growth coefficient, μ, assuming a constant kinetic rate parameter, V_o.

2. Experimental methods

For the electrostatic levitation experiments, Fe–Co samples were prepared at 30, 40, and 50 at.% cobalt, from 99.995% pure iron, and 99.95% pure cobalt, by arc-melting the components under an argon atmosphere, such that they had a mass of approximately 40 mg (~ 2 mm diameter). They were processed via ESL, where the negatively charged sample was contained within a vacuum chamber (evacuated to 10^{-9} mbar), between a negatively charged lower plate, and a positively charged upper plate. The Fe–Co phase diagram is given in Fig. 1.

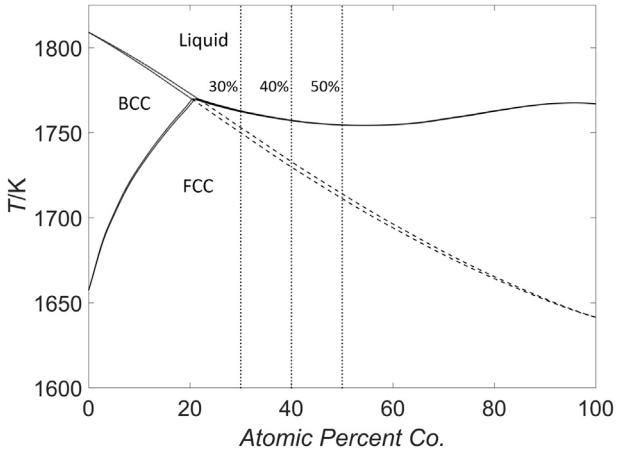

Fig. 1. Fe–Co phase diagram from Rodriguez and Matson [1]. — Equilibrium phase lines; –– Metastable BCC and Liquid lines; ····· Tested compositions.

The sample was then melted, allowed to cool radiatively, and then solidify. An article by Rogers and SanSoucie [11] gives a full description of the experimental setup. The solidification was monitored with a Phantom V7.1 high-speed camera, which was operating at 30,000–40,000 frames per second at 128 × 128 image resolution. The location of the sample was determined by positioning lasers, and the electrostatic field was adjusted accordingly. The temperature of the samples was monitored with a Mikron MI-GA140 single color pyrometer, which has a 1.45 μm–1.8 μm wavelength range, and was operating at 16 Hz. The pyrometer accuracy is ± 0.3% of reading in °F + 1.8 °F for T < 2732 °F (1773 K), and ± 0.5% of reading in F for T > 2732 °F (1773 K). The pyrometer was calibrated with a Mikron M390 blackbody generator [12].

Electromagnetic levitation experiments were carried out at DLR Cologne. Fe–Co alloys were arc melted from 99.995 at.% pure Fe and Co under high purity (6 N) 1000 mbar Ar atmosphere. The sample mass was about 1 g corresponding to a sphere of typically 6.5 mm in diameter. The vacuum chamber of the levitation facility was evacuated to 10^{-6} mbar and then filled with high purity (6 N) He to 400 mbar. The sample was levitated and inductively heated in a coil consisting of water-cooled Cu-windings carrying an alternating current of frequency in the range of 350 kHz. Samples were melted and then cooled by a He gas stream in several cycles. The temperature-time profile was measured by an IMPAC ISR 12-CO single color pyrometer at 100 Hz with an operating range of 0.8–1.05 μm. Rapid solidification during recalescence of the undercooled melt was recorded with a Photron Fastcam SA5 high-speed video camera at a rate of 75,000 fps and a resolution of 320 × 264 pixels. A comprehensive description of the levitation facility is given elsewhere [13].

The temperature of the sample was measured with a pyrometer, however it is possible to increase the temporal resolution of the measurement by utilizing high-speed video data. The grayscale intensity of a given pixel can be correlated to a temperature value if temperatures of the undercooled liquid and the stable phase are known. An article by Burke et al. [12] contains a more rigorous investigation of the use of a broad-band pyrometer as a primary temperature measurement device. Fig. 2 shows images of progression of solidification, a plot of pixel intensity at the nucleation point, and a linear fit relating temperature to intensity. In this case, it is evident that there is a linear correlation between the known temperatures and pixel intensity values, and that facilitates a simple conversion from pixel intensity to temperature.

3. Analysis

The dendrite growth velocity modeling is fully described by Lipton, Kurz, and Trivedi (LKT) [9], with the effects of kinetic undercooling given by Boettinger, Coriell, and Trivedi (BCT) [10]. Therefore, this section will include a brief overview of the analysis. A list of symbols and descriptions is given in Appendix A.

The undercooling is given by:

$$\Delta T = \Delta T_T + \Delta T_R + \Delta T_C + \Delta T_K \tag{1}$$

where ΔT_T is the thermal undercooling, ΔT_R is the curvature undercooling, ΔT_C is the solutal undercooling, and ΔT_K is the kinetic undercooling. All values of undercooling are with respect to the phase of interest. The thermal undercooling, ΔT_T, is given in Equation (2).

$$\Delta T_T = \frac{\Delta H_f}{\Omega C_P^L} Iv(P_T) \tag{2}$$

Ω is the molar volume, C_P^L is the heat capacity of the undercooled

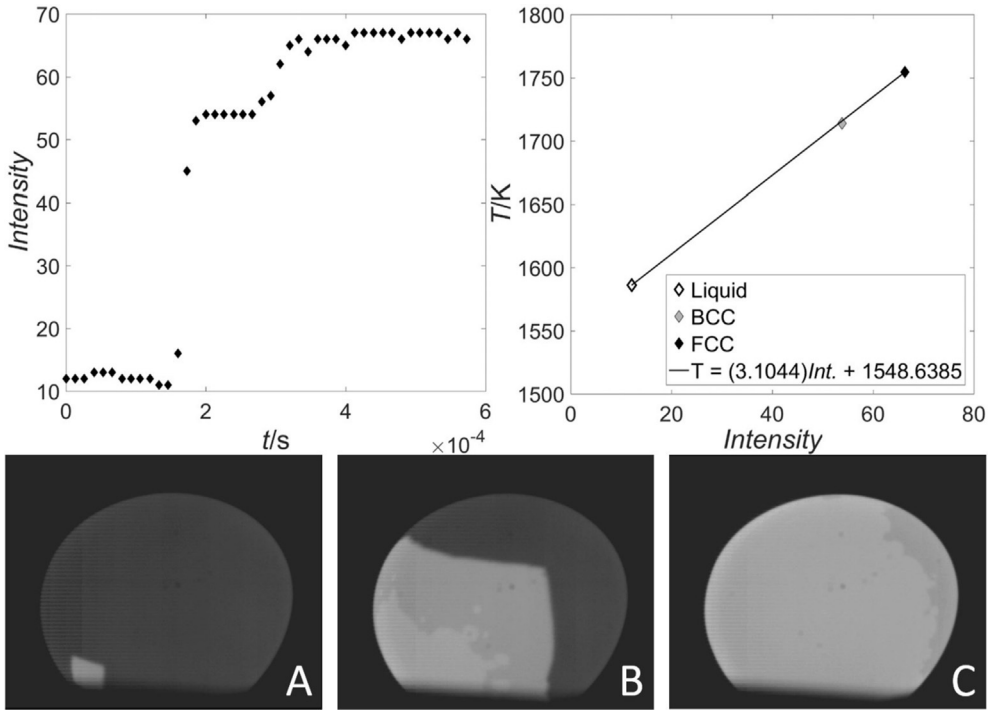

Fig. 2. Images of the progression of solidification of a Fe–50 at.% Co sample processed in EML (A–C), the corresponding plot of pixel intensity at the nucleation point (Top Left), and a linear fit relating temperature to intensity (Top Right). Image A shows the onset of growth of the metastable δ–phase, B shows the initial growth of the stable γ–phase through the mushy zone, and C shows nearly completed growth of the γ–phase.

liquid, ΔH_f is the heat of fusion, and $Iv(P_T)$ is the Ivantsov function of the thermal Péclet number, P_T.

The definition of the Ivantsov function is given in Equation (3).

$$Iv(P_x) = P_x e^{P_x} E_1(P_x) \tag{3}$$

$E_1(P_x)$ is the exponential integral function, where the argument P_x refers to the thermal or solutal Péclet number.

$$P_T = \frac{VR}{2\alpha} \tag{4}$$

V is the solidification velocity, α is the thermal diffusivity, and R is the radius of the dendrite tip. The undercooling due to curvature, ΔT_R, is shown in Equation (5).

$$\Delta T_R = 2\frac{\Gamma}{R} \tag{5}$$

Γ is the Gibbs-Thomson coefficient, given by:

$$\Gamma = \frac{\sigma}{\Delta S_f} \tag{6}$$

where ΔS_f is the entropy of fusion, and σ is the solid-liquid interfacial energy. The solutal undercooling is given in Equation (7).

$$\Delta T_C = m_L C_o \left[1 - \frac{m_v}{m_L[1-(1-k)Iv(P_C)]}\right] \tag{7}$$

m_L is the slope of the liquidus line from the equilibrium phase diagram, m_v is the correction for the kinetic effect on the phase diagram slope, C_o is the solute concentration, k is the velocity-dependent partitioning coefficient according to the model by Aziz and Kaplan [14], and P_C is the solutal Péclet number.

$$P_C = \frac{VR}{2D_o} \tag{8}$$

$$m_v = m_L\left[\frac{1+[k_e - k(1-ln(k/k_e))]}{1-k_e}\right] \tag{9}$$

k_e is the equilibrium partition coefficient.

$$k = \frac{k_e + V/V_d}{1-(1-k_e)X_o + V/V_d} \tag{10}$$

X_o is the initial solute atomic fraction, and V_d is the atomic diffusive speed at the solid-liquid interface, shown in Equation (11).

$$V_d = D_o/a_o \tag{11}$$

D_o is the solute diffusivity, and a_o is the atomic spacing in the liquid. The kinetic undercooling, ΔT_K, is given in Equation (12).

$$\Delta T_K = V/\mu \tag{12}$$

μ is the kinetic growth coefficient, shown in Equation (13).

$$\mu = \frac{\Delta H_f V_o}{\bar{R}T_m^2} \tag{13}$$

T_m is the melting temperature, $\bar{R}$ is the universal gas constant, and V_o is the kinetic rate parameter, where $V_d<V_o<V_S$. V_S is the speed of sound through the liquid, and V_d is the diffusive speed defined above. The undercooling equation provides a relationship for VR, however, a second equation is necessary in order to solve for the unique value of velocity at a given undercooling. The second equation comes from the dendrite tip selection condition, as shown in Equation (14).

$$\frac{\Gamma}{\sigma^* R^2} = m_v G_C \xi_C - \left[\overline{K_S} G_S \xi_S + \overline{K_L} G_L \xi_L\right] \quad (14)$$

σ^* is the stability parameter, G_C is the solute gradient in the liquid, G_S and G_L are the temperature gradients in the solid and liquid, respectively. ξ_C is the solute stability function, dependent on the solutal Péclet number, while ξ_S and ξ_L are the stability functions, dependent on the thermal Péclet numbers for the solid and liquid, respectively. $\overline{K_S}$ and $\overline{K_L}$ are the weighted conductivities of the solid and liquid, given as $\overline{K_S} = K_S/(K_S + K_L)$ and $\overline{K_L} = K_L/(K_S + K_L)$. For an isothermal dendrite $G_S = 0$. G_L and G_C are given in Equations 15 and 16.

$$G_L = -\frac{V\Delta H_f}{\alpha C_P^L \Omega} \quad (15)$$

$$G_C = -\frac{VC_o(1-k)}{D_o[1-(1-k)Iv(P_C)]} \quad (16)$$

Assuming $\alpha_S = \alpha_L = \alpha$ and $K_S = K_L$, then combining Equations 15 and 16 with the stability condition, Equation (14), and solving for R, produces Equation (17). The stability functions, ξ_L and ξ_C are shown in Equations (18) and (19).

$$R = \frac{\Gamma/\sigma^*}{\frac{P_T \Delta H_f}{\Omega C_P^L}\xi_L - \frac{2m_v C_o(1-k)P_C}{1-(1-k)Iv(P_C)}\xi_C} \quad (17)$$

$$\xi_L = 1 - \frac{1}{\sqrt{1+\frac{1}{\sigma^* P_T^2}}} \quad (18)$$

$$\xi_C = 1 + \frac{2k}{1-2k-\sqrt{1+\frac{1}{\sigma^* P_C^2}}} \quad (19)$$

Langer and Müller-Krumbhaar [15] proposed a marginal stability condition, where σ^* was set to be equal to $1/4\pi^2$, which Trivedi and Kurz [16] applied within a planar interface perturbation analysis. Solvability theory considers solid-liquid interface energy anisotropy, where the value of the stability parameter takes the form $\sigma^* = \sigma_o \varepsilon_C^{7/4}$. σ_o is a constant, and ε_C corresponds to the interface energy anisotropy [17,18]. When external flow is considered, the stability parameter becomes a function of the flow velocity, U, where $\sigma^* = \sigma_o \varepsilon_C^{7/4} f(U)$[19,20].

As previously stated, there were no observed effects of melt convection on primary growth kinetics. Therefore, external flow considerations were neglected within the stability parameter. In general, the application of the marginal stability criterion within the perturbation analysis predicts experimental results well, and reduces the number of unknowns and adjustable parameters within the analysis. For these reasons, σ^* was chosen to be equal to $1/4\pi^2$ within the current work. Table 1 shows the thermophysical property values that were used in the analysis.

4. Results and discussion

Table 2 shows the average growth velocity of the stable phase through the mushy zone, $\overline{V}_{\gamma\delta}$, as well as the kinetic coefficient, μ, which was used in the dendrite growth analyses. The error margins given for $\overline{V}_{\gamma\delta}$ were calculated at a 95% confidence level.

From Equation (13), μ is seen to vary with $\Delta H_f/T_m^2$. Therefore, as the alloy composition shifts μ should shift in accordance with the change in $\Delta H_f/T_m^2$ for a given solid phase. In this case, that value changes very little, which is why μ is similar for all three alloy compositions.

Figs. 3–5 show the experimental growth velocity results from the current work, as well as those from Dolan [29] and Hermann et al. [4]. In some cases, after the metastable phase nucleated, the stable phase would nucleate within the mushy zone formed during primary solidification and grow fast enough to outgrow the metastable phase and escape into the undercooled liquid. In those cases, it was possible to estimate the solid-liquid growth velocity for both solid phases as well as the velocity of the stable phase growing into the mushy zone. The results are displayed as a function of the undercooling relative to the melting point of the stable phase. For example, for the Fe–40 at.% Co alloy, the thermal driving force is calculated from the difference between the melting points:

$$\Delta T_{\gamma\delta} = T_\gamma - T_\delta = 1757 - 1733 = 24K. \quad (20)$$

For an undercooling of 100 K relative to the stable phase, the undercooling relative to the metastable phase is 76 K. There are no growth velocity measurements of either the metastable phase into

Table 1
Thermophysical property values used in the solidification analysis.

Properties	$Fe_{70}Co_{30}$	$Fe_{60}Co_{40}$	$Fe_{50}Co_{50}$
a_o[a] (m) [21]	2.358E-10	2.354E-10	2.35E-10
α[a] (m^2/s) [22]	5.46E-06	5.36E-06	5.29E-06
C_o (at.%)	30	40	50
$C_P^{L,\gamma}\|C_P^{L,\delta}$ (J/m^3-K) [1]	5749190 | 5712909	5796451 | 5704510	5822432 | 5666976
D_o (m^2/s) [23]	4.7E-9	4.7E-9	4.7E-9
$\Delta H_\gamma\|\Delta H_\delta$ (J/mol) [1]	14098 | 10999	14083 | 10767	14154 | 10795
$k_e^\gamma\|k_e^\delta$[1]	0.977 | 0.949	0.989 | 0.96	0.997 | 0.969
$m_L^\gamma\|m_L^\delta$ (K/at.%) [1]	−0.69 | -1.99	0.45 | -1.98	0.13 | -1.85
$T_\gamma\|T_\delta$ (K) [1]	1763 | 1753	1757 | 1733	1754 | 1714
$\Delta T_{\gamma\delta}$ (K) [1]	10	24	40
σ_γ[b]$\|\sigma_\delta$[b] (J/m^2) [24]	0.319 | 0.206	0.319 | 0.206	0.319 | 0.206
η (Pa-s) [25]	0.005919	0.005808	0.005698
ρ_S[a]$\|\rho_L$ (kg/m^3)	7612 [26,27]| 7242 [28]	7718 [26,27]| 7352.53 [28]	7824 [26,27]| 7423.47 [28]
$\Delta S_\gamma\|\Delta S_\delta$ (J/m^3-K) [1]	1020485 | 801219	1032396 | 801030	1043547 | 815419
$V_o^\gamma\|V_o^\delta$ (m/s)	550 | 350	550 | 350	550 | 350
V_S[a][21]$\|V_d$ (m/s)	4307 | 19.9	4276 | 20	4245 | 20
Ω_S[a]$\|\Omega_L$ (m^3/mol)	7.4577 E−6 | 7.8384 E−6	7.3953 E−6 | 7.76335 E−6	7.3346 E−6 | 7.73076 E−6
X_o (at. Fraction)	0.3	0.4	0.5

[a] Indicates that ideal mixing was assumed and that the values were obtained based on the atomic composition of the alloy.
[b] Values for pure iron were used.

Table 2
Values of $\overline{V}_{\gamma\delta}$ and μ for each composition tested. The ± error margins were calculated at a 95% confidence level.

Properties	$Fe_{70}Co_{30}$	$Fe_{60}Co_{40}$	$Fe_{50}Co_{50}$
$\mu_{\gamma L}\|\mu_{\delta L}$ (m/s·K)	0.300 | 0.151	0.302 | 0.151	0.304 | 0.155
$\overline{V}_{\gamma\delta}$ (m/s)	1.6 ± 0.45	2.4 ± 0.23	4.9 ± 0.27
Standard Deviation (m/s)	0.76	0.64	1.42
Num. $V_{\gamma\delta}$ Data Points	11	29	104

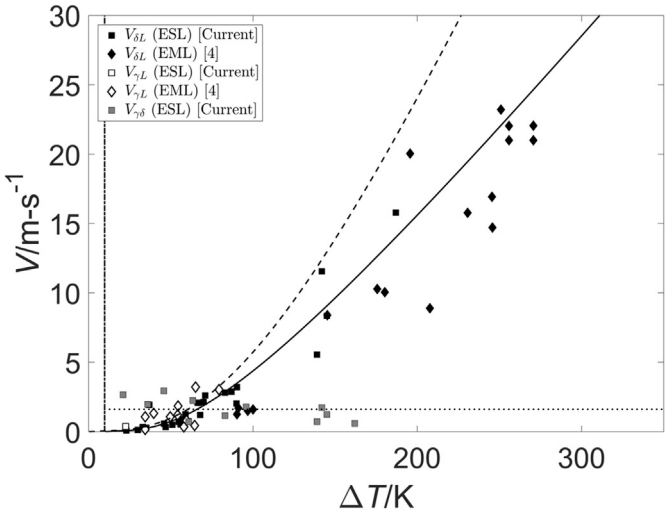

Fig. 3. Growth velocity of Fe–30 at.% Co as a function of undercooling, including experimental results from ESL testing as well as the results of the LKT/BCT [9,10] analysis. — $V_{\delta L}$, $\mu = 0.151$ m/s·K; —— $V_{\gamma L}$, $\mu = 0.300$ m/s·K; ••••••• $\overline{V}_{\gamma\delta} = 1.6$ m/s, is the averaged value of the available experimental data points of $V_{\gamma\delta}$; -•-• $\Delta T_{\gamma\delta} = 10$ K, marks the temperature difference between the stable phase and the metastable phase [1].

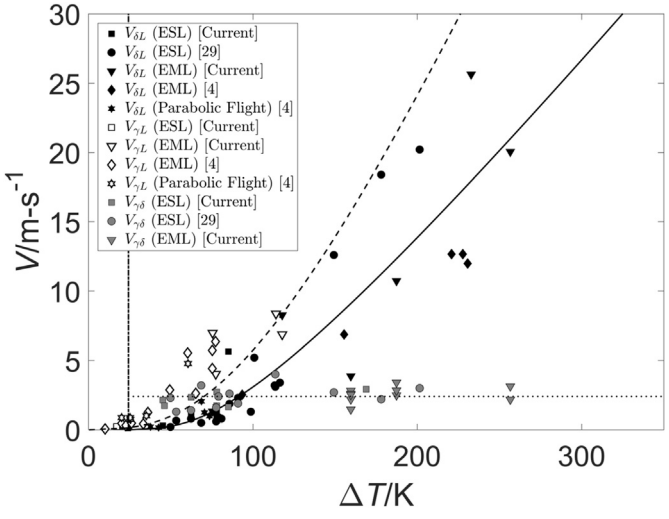

Fig. 4. Growth velocity of Fe–40 at.% Co as a function of undercooling, including experimental results from ESL and EML testing as well as the results of the LKT/BCT [9,10] analysis. — $V_{\delta L}$, $\mu = 0.151$ m/s·K; —— $V_{\gamma L}$, $\mu = 0.302$ m/s·K; ••••••• $\overline{V}_{\gamma\delta} = 2.4$ m/s, is the averaged value of the available experimental data points of $V_{\gamma\delta}$; -•-• $\Delta T_{\gamma\delta} = 24$ K, marks the temperature difference between the stable phase and the metastable phase [1].

liquid, or the stable phase into the mushy zone if the underooling is less than 24 K, as there can be no double recalescence.

The curves representing the growth of the solid phases through the liquid are the results of the dendrite growth analyses assuming

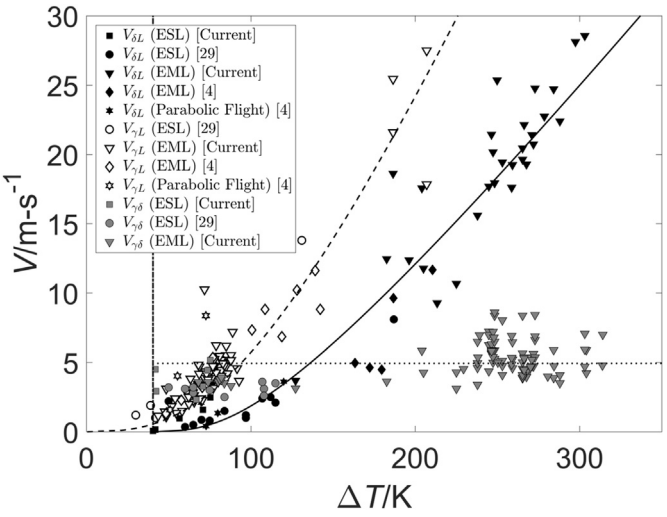

Fig. 5. Growth velocity of Fe–50 at.% Co as a function of undercooling, including experimental results from ESL and EML testing as well as the results of the LKT/BCT [9,10] analysis. — $V_{\delta L}$, $\mu = 0.155$ m/s·K; —— $V_{\gamma L}$, $\mu = 0.304$ m/s·K; ••••••• $\overline{V}_{\gamma\delta} = 4.9$ m/s, is the averaged value of the available experimental data points of $V_{\gamma\delta}$; -•-• $\Delta T_{\gamma\delta} = 40$ K, marks the temperature difference between the stable phase and the metastable phase [1].

a kinetic rate parameter of $V_o^{\delta} = 350$ m/s-K for the δ–phase, and $V_o^{\gamma} = 550$ m/s-K for the γ–phase. For a constant value of V_o for each phase, the results of the dendrite growth analyses match sufficiently well with the experimental data. This indicates that it is reasonable to assume that V_o is constant for a given phase within an alloy system if $\Delta H_f/T_m^2$ does not vary significantly within the system, or within the composition range of interest.

The velocity of the solid phases growing into undercooled liquid, as well as the stable phase growing into the mushy zone, were found to be independent of melt convection. This is because the growth velocity is much greater than the melt convection velocity, particularly at higher undercoolings [6]. In the case of the γ–phase growing through the mushy zone, it is unlikely that there will be significant stirring due to the presence of the dendritic structure of the metastable phase.

The mushy zone velocity is greater than that of the stable phase growing through undercooled liquid at the critical undercooling, $\Delta T_{\gamma\delta}$, and it is independent of the initial undercooling, but varies with cobalt concentration. The γ–phase mushy-zone growth velocity becomes larger as the cobalt concentration is increases because the difference between melting temperatures of the δ–phase and γ–phase increases. Matson and Hyers [30] previously addressed this observation within an adiabatic remelt model. In the remelt model, some portion of the pre-existing metastable phase is remelted, absorbing the heat of fusion. This remelting is accounted for with an effective heat capacity of the growth environment which is greater than the heat capacity of the liquid by itself. Given that the effective heat capacity is greater than the liquid heat capacity, and that the thermal driving potential, $\Delta T_{\gamma\delta}$, is constant for a given alloy composition, it is logical that the growth velocity of the stable phase through the mushy zone will be constant, and greater than that of the solid phase growing through liquid at the same undercooling, $\Delta T_{\gamma\delta}$.

The experimental results show no significant effects of a transition from solutal growth to the kinetically limited regime, which have previously been observed in other alloy systems [31–33]. This behavior is expected because both the δ–phase, and γ–phase, exhibit very little partitioning.

From the measured velocities it is clear that the growth of stable

γ−phase into the undercooled liquid is faster than that of the metastable δ−phase at a given undercooling. This is, in part, due to the fact that the undercooling relative to the metastable phase represents only a fraction of the total undercooling. The undercooled melt solidifies primarily into the metastable phase although its growth rate is smaller than that of the stable counterpart. Thus, growth of competing phases can be excluded as the mechanism for phase selection. Primary solidification of the metastable δ−phase phase must therefore be determined by preferred nucleation.

5. Conclusions

We have provided new experimental results of the growth velocity of the stable phase into the mushy zone for various Fe−Co alloys. Based on the experimental results, there are several key takeaways: 1) The velocity of the stable phase growing into the mushy zone is greater than that of the stable phase growing into undercooled liquid at the critical undercooling. 2) The growth velocities of the solid phases growing through undercooled liquid are unaffected by liquid flow velocity. 3) There are no significant observable effects of the transition from solutal growth to kinetically limited growth.

The results of the dendrite growth analysis indicate that it is reasonable to assume that the kinetic rate parameter, V_o, is constant for a given phase within an alloy system if $\Delta H_f/T_m^2$ does not vary significantly within the system, or within the composition range of interest. It is unclear whether this assumption will be valid in the event that $\Delta H_f/T_m^2$ varies significantly with changes in alloy composition, however, that is only likely to be the case when the alloy contains very dissimilar components in moderate quantities. This is a particularly useful finding which will allow researchers to estimate growth conditions in new alloys by extrapolating from previously known data.

Acknowledgments

We would like to thank Glenn Fountain and Trudy L. Allen for technical assistance at NASA Marshall Space Flight Center (MSFC). The work at Tufts University was partially funded by NASA, under grant numbers NNX10AV27G, NNX14AB74G, and NNX16AB59G. Financial support from the European Space Agency for the work at DLR, under contract number 4200014980, is also gratefully acknowledged.

Appendix A

Nomenclature

Symbols	Description
a_o	Atomic spacing in liquid.
α	Thermal diffusivity.
C_o	Solute concentration.
C_P^L	Heat capacity.
D_o	Solute diffusivity.
G_L	Temperature gradient in the liquid.
G_S	Temperature gradient in the solid.
Γ	Gibbs-Thompson coefficient.
ΔH_f	Heat of fusion.
k	Non-equilibrium partition correction.
k_e	Equilibrium partition coefficient.
μ	Kinetic growth coefficient.
m_L	Equilibrium liquidus slope.
m_v	Non-equilibrium liquidus slope correction.
P_T	Thermal Peclet number.
P_C	Solutal Peclet number.
R	Dendrite tip radius.
$\overline{R}$	Universal gas constant.
σ	Solid liquid interface energy.
σ^*	Tip radius stability constant.
ΔS_f	Entropy of fusion.
T_δ	δ−phase liquidus temperature
T_γ	γ−phase liquidus temperature
$\Delta T_{\gamma\delta}$	$T_\gamma - T_\delta$
ΔT	Bath undercooling.
ΔT_C	Solutal undercooling.
ΔT_K	Kinetic undercooling.
ΔT_R	Curvature undercooling.
ΔT_T	Thermal undercooling.
Ω	Molar volume.
V	Tip velocity.
V_d	Atomic diffusive speed.
$V_{\delta L}$	Growth velocity of the δ−phase into undercooled liquid.
$V_{\gamma L}$	Growth velocity of the γ−phase into undercooled liquid.
$V_{\gamma\delta}$	Growth velocity of the γ−phase into the mushy zone.
V_o	Kinetic rate parameter.
V_S	Speed of sound though the liquid.
ξ_L	Tip radius stability parameter. Dependent on P_T of liquid.
ξ_S	Tip radius stability parameter. Dependent on P_T of solid.
ξ_C	Tip radius stability parameter. Dependent on P_C.

References

[1] Justin E. Rodriguez, Douglas M. Matson, Thermodynamic modeling of the solidification path of levitated Fe−Co alloys, Calphad 49 (June 2015) 87−100.
[2] R. Hermann, W. Löser, Growth kinetics of undercooled Fe−Co melts, J. Magnetism Magnetic Mater. 242−245 (1) (April 2002) 285−287.
[3] R. Hermann, W. Löser, G. Lindenkreuz, A. Diefenbach, W. Zahnow, W. Dreier, Th Volkmann, D. Herlach, Metastable phase formation in undercooled Fe−Co melts, Mater. Sci. Eng. A 375−377 (July 2004) 507−511.
[4] R. Hermann, W. Löser, H.G. Lindenkreuz, W. Yang-Bitterlich, Ch Mickel, A. Diefenbach, S. Schneider, W. Dreier, Metastable phase formation in undercooled Fe-Co melts under terrestrial and parabolic flight conditions, Microgravity - Sci. Technol. 19 (1) (December 2007) 5−10.
[5] M. Asta, C. Beckermann, A. Karma, W. Kurz, R. Napolitano, M. Plapp, G. Purdy, M. Rappaz, R. Trivedi, Solidification microstructures and solid-state parallels: recent developments, future directions, Acta Mater. 57 (4) (February 2009) 941−971.
[6] Robert W. Hyers, Douglas M. Matson, Kenneth F. Kelton, Jan R. Rogers, Convection in containerless processing, Ann. N. Y. Acad. Sci. 1027 (1) (November 2004) 474−494.
[7] Mingjun Li, Xin Lin, Guangsheng Song, Gencang Yang, Yaohe Zhou, Microstructure evolution and metastable phase formation in undercooled Fe−30 at.% Co melt, Mater. Sci. Eng. A 268 (1−2) (August 1999) 90−96.
[8] Douglas M. Matson, David J. Fair, Robert W. Hyers, Jan R. Rogers, Contrasting electrostatic and electromagnetic levitation experimental results for transformation kinetics of steel alloys, Ann. N. Y. Acad. Sci. 1027 (1) (November 2004) 435−446.
[9] J. Lipton, W. Kurz, R. Trivedi, Rapid dendrite growth in undercooled alloys, Acta Metall. 35 (4) (1987) 957−964.
[10] W.J. Boettinger, S.R. Coriell, R. Trivedi, Application of dendritic growth theory to the interpretation of rapid solidification microstructures, Rapid Solidif. Process. Princ. Technol. IV (1988) 13.
[11] Jan Rogers, Michael Sansoucie, Containerless processing studies in the msfc electrostatic levitator, in: 50th AIAA Aerospace Sciences Meeting Including the New Horizons Forum and Aerospace Exposition, American Institute of Aeronautics and Astronautics, January 2012.
[12] James M. Burke, Andrew J. Mueller, David J. Fair, Douglas M. Matson, Application of em levitation processing: fundamental studies of steel rapid solidification. In materials science and technology, Assoc. Iron Steel Technol. (2005) 71−78.
[13] D.M. Herlach, Containerless undercooling and solidification of pure metals, Annu. Rev. Mater. Sci. 21 (1) (1991) 23−44.
[14] Michael J. Aziz, Theodore Kaplan, Continuous growth model for interface motion during alloy solidification, Acta Metall. 36 (8) (August 1988) 2335−2347.
[15] J.S. Langer, H. Müller-Krumbhaar, Theory of dendritic growth—I. Elements of a stability analysis, Acta Metall. 26 (11) (1978) 1681−1687.
[16] R. Trivedi, W. Kurz, Morphological stability of a planar interface under rapid solidification conditions, Acta Metall. 34 (8) (August 1986) 1663−1670.
[17] David A. Kessler, Herbert Levine, Velocity selection in dendritic growth, Phys. Rev. B 33 (11) (June 1986) 7867−7870.
[18] David Bensimon, Pierre Pelcé, Boris I. Shraiman, Dynamics of curved fronts and pattern selection, J. de Physique 48 (12) (1987) 2081−2087.

[19] Ph Bouissou, P. Pelcé, Effect of a forced flow on dendritic growth, Phys. Rev. A 40 (11) (December 1989) 6673–6680.
[20] Dieter M. Herlach, Non-equilibrium solidification of undercooled metallic melts, Metals 4 (2) (June 2014) 196–234.
[21] Takamichi Iida, Roderick IL. Guthrie, The Physical Properties of Liquid Metals, Oxford University Press Inc., 1993.
[22] Tsuyoshi Nishi, Hiroyuki Shibata, Yoshio Waseda, Hiromichi Ohta, Thermal conductivities of molten iron, cobalt, and nickel by laser flash method, Metallurgical Mater. Trans. A 34 (12) (December 2003) 2801–2807.
[23] D.W. Morgan, J.A. Kitchener, Solutions in liquid iron. Part 3:—Diffusion of cobalt and carbon, Trans. Faraday Soc. 50 (1954) 51–60.
[24] D.Y. Sun, M. Asta, J.J. Hoyt, M.I. Mendelev, D.J. Srolovitz, Crystal-melt interfacial free energies in metals: fcc versus bcc, Phys. Rev. B 69(2) (020102) (January 2004).
[25] Yuzuru Sato, Koji Sugisawa, Daisuke Aoki, Tsutomu Yamamura, Viscosities of Fe–Ni, Fe–Co and Ni–Co binary melts, Meas. Sci. Technol. 16 (2) (February 2005) 363.
[26] Kenneth C. Mills, Recommended Values of Thermophysical Properties for Selected Commercial Alloys, Woodhead Publishing, 2002.
[27] Gernot Pottlacher, High temperature thermophysical properties of 22 pure metals, Keiper (2010) 152. Graz, Austria, ISBN: 978-3-9502761-6-9.
[28] Jonghyun Lee, Justin E. Rodriguez, Robert W. Hyers, Douglas M. Matson, Measurement of density of Fe-Co alloys using electrostatic levitation, Metallurgical Mater. Trans. B 46 (6) (August 2015) 2470–2475.
[29] Jackson R. Dolan, Application of the Adiabatic Remelt Model to the Solidification of Undercooled Iron-cobalt Alloys, Tufts University, United States – Massachusetts, 2012. M.S.
[30] D.M. Matson, R.W. Hyers, Adiabatic remelting of the mushy-zone during rapid solidification, Philos. Mag. 86 (24) (August 2006) 3795–3807.
[31] K. Eckler, R.F. Cochrane, D.M. Herlach, B. Feuerbacher, M. Jurisch, Evidence for a transition from diffusion-controlled to thermally controlled solidification in metallic alloys, Phys. Rev. B 45 (9) (March 1992) 5019–5022.
[32] P.K. Galenko, S. Reutzel, D.M. Herlach, D. Danilov, B. Nestler, Modelling of dendritic solidification in undercooled dilute Ni–Zr melts, Acta Mater. 55 (20) (December 2007) 6834–6842.
[33] H. Hartmann, P.K. Galenko, D. Holland–Moritz, M. Kolbe, D.M. Herlach, O. Shuleshova, Nonequilibrium solidification in undercooled Ti45al55 melts, J. Appl. Phys. 103(7) (073509) (April 2008).